

2013

BABES-BOLYAI

UNIVERSITY

FACULTY OF PHYSICS

PhD student: Ramona Ioana Chelcea

Scientific supervisor: Prof. dr. Eugen Culea



PhD Thesis

Abstract

THE INVESTIGATION AND MODELING OF
STRUCTURAL PROPERTIES OF SOME VITREOUS
AND VITROCERAMICS GERMANATE SYSTEMS

Cluj Napoca 2013

Content

Introduction

1. Chapter 1:

Methods for preparation and investigation of glasses

- 1.1 Obtaining oxide glasses
- 1.2 Methods for glasses attainment
 - 1.2.1 Melt and quenching method
 - 1.2.2 Shock exposure of crystalline material method
 - 1.2.3 Action of neutrons method
 - 1.2.4 Thin film deposition method
 - 1.2.5 Sol-gel method
- 1.3 Methods of investigation of glasses materials
 - 1.3.1 UV-VIS spectroscopy
 - 1.3.2 IR spectroscopy
 - 1.3.3 Electronic paramagnetic resonance
 - 1.3.4 X ray and neutrons diffraction
 - 1.3.5 Density measurements

Bibliography

2. Chapter 2:

Presentation of some germanate systems studied in literature

- 2.1 Vitreous system $[0.95(\text{GeO}_2 \times \text{PbO}).0.05\text{Al}_2\text{O}_3]$
- 2.2 Vitreous system $20\text{Fe}_2\text{O}_3 \cdot 80[3\text{B}_2\text{O}_3(1-x)\text{PbO}_x\text{GeO}_2]$
- 2.3 Vitreous system $5\text{Al}_2\text{O}_3 \cdot [x\text{Gd}_2\text{O}_3 \cdot (100-x)(7\text{GeO}_2 \cdot 3\text{PbO})]$
- 2.4 Vitreous system $7\text{GeO}_2 \cdot 3\text{PbO}_2$ and $7\text{GeO}_2 \cdot 3\text{PbO}$ with Eu and Gd ions

Bibliography

3. Chapter 3:

The computational modeling of vitreous systems properties

- 3.1 Approximations used in molecular modeling
 - 3.1.1. Born – Oppenheimer

- 3.1.2. LCAO
 - 3.1.3. Hartree – Fock or The Self Consistent Field
 - 3.2. Molecular Modeling methods
 - 3.2.1. Molecular Mechanics
 - 3.2.2. Semi – Empirical
 - 3.2.3. Ab-Initio
 - 3.2.4. DFT (Density Functional Theory)
 - 3.3 Molecular Modeling of local structure of some germanate systems
 - 3.3.1. Molecular modeling of $[\text{GeO}_2 \cdot \text{V}_2\text{O}_5]$
 - 3.3.2 Molecular modeling of $\text{CuO} \cdot 7\text{GeO}_2 \cdot 3\text{PbO}_2$
 - 3.3.3 Molecular modeling of $20\text{MoO}_3 \cdot 80[7\text{GeO}_2 \cdot 3\text{PbO}]$
 - 3.3.4 Molecular modeling of $20\text{WO}_3 \cdot 80[7\text{GeO}_2 \cdot 3\text{PbO}]$
- Bibliography

4. Chapter 4:

The preparation and investigation of some germanate glasses

- 4.1 Introduction
- 4.2 Structural studies of $x\text{CuO} \cdot (100 - x)[7\text{GeO}_2 \cdot 3\text{PbO}_2]$
 - 4.2.1. FT-IR measurements
 - 4.2.2 UV-VIS measurements
 - 4.2.3 Density measurements
 - 4.2.4. RPE measurements
 - 4.2.5. Conclusions
- 4.3 Structural studies of $x\text{CuO} \cdot (100-x)[7\text{GeO}_2 \cdot 3\text{PbO}_2 \cdot 0.05\text{Al}_2\text{O}_3]$
 - 4.3.1. FT-IR measurements
 - 4.3.2. UV-VIS measurements
 - 4.3.3 RPE measurements
 - 4.3.4 Conclusions
- 4.4 Structural studies of $x\text{Fe}_2\text{O}_3 \cdot (100 - x)[7\text{GeO}_2 \cdot 3\text{PbO}]$
 - 4.4.1 X-ray diffraction measurements
 - 4.4.2 FT-IR measurements
 - 4.4.3 UV-VIS measurements
 - 4.4.4 Density measurements
 - 4.4.5. Conclusions

- 4.5 Structural study of ternary iron-lead-germanate glass ceramics
 - 4.5.1 X-ray diffraction measurements
 - 4.5.2 FT-IR measurements
 - 4.5.3 UV-VIS measurements
 - 4.5.4 Conclusions
- 4.6 Structural studies of $x\text{MoO}_3 \cdot (100-x)[7\text{GeO}_2 \cdot 3\text{PbO}]$
 - 4.6.1 X-ray diffraction measurements
 - 4.6.2 Density measurements
 - 4.6.3 FT-IR measurements
 - 4.6.4 UV-VIS measurements
 - 4.6.5 RPE measurements
 - 4.6.6 Conclusions
- 4.7 Structural studies of $x\text{WO}_3 \cdot (100-x)[7\text{GeO}_2 \cdot 3\text{PbO}]$
 - 4.7.1 X-ray diffraction measurements
 - 4.7.2 FT-IR measurements
 - 4.7.3 UV-VIS measurements
 - 4.7.4 RPE measurements
 - 4.7.5 Conclusions
- 4.8 Structural studies of $x\text{Gd}_2\text{O}_3 \cdot (100-x)[\text{TeO}_2 \cdot \text{GeO}_2]$
 - 4.8.1 FT-IR measurements
 - 4.8.2 UV-VIS measurements
 - 4.8.3 RPE measurements
 - 4.8.4 Conclusions
- 4.9 Structural studies of $x\text{Gd}_2\text{O}_3 \cdot (100-x)[\text{GeO}_2 \cdot \text{V}_2\text{O}_5]$
 - 4.9.1 Density measurements
 - 4.9.2 FT-IR measurements
 - 4.9.3 UV-VIS measurements
 - 4.9.4 Conclusions

Bibliography

Selective conclusions

Keywords:

Vitros and vitroceramics systems, metallic and rare earth oxides, molecular modeling, RPE, FT-IR, UV-VIS spectroscopies, X-ray diffraction, density measurements.

INTRODUCTION

Lately research in materials science have taken a great extent, perhaps for the need for the industry to develop and acquire new types of materials techniques and modern technology, materials that have a wide practical application. Currently, it follows the acquisition of new materials applied in electronics, electrical, construction, medicine, pharmacy, etc., and obtaining materials with the size from nanoparticles to finished products of large dimensions. From a practical standpoint besides the problem of obtaining these new types of materials are also the knowledge of their structure because their properties of interest for certain types of applications depend and may be influenced by their structure.

The studies on oxide materials structure are performed using various experimental techniques for determining the types of bonds and coordination between different numbers of atoms of the investigated substance. An inconvenience is that, in practice, most of the time only one experimental technique allows the determination of a part of the structural features of the investigated materials. Thus, we need to use several complementary experimental techniques for a complete investigation of materials and determination of the properties of interest for specific applications.

Lead-germanate glasses have been investigated more carefully because of their important properties, such as good chemical and mechanical stability, a higher temperature than the glass transition. Such glasses offer opportunities for different applications in optoelectronics and telecommunications. The lead-

germanate glasses are technologically important due to their potential use as glasses with low optical loss in the infrared domain. In addition, their study is interesting because such materials can be obtained easily in the form of fibers so are well suitable to be used in telecommunications and other applications of electromagnetic energy transmission systems.

In this thesis, I proposed to prepare and to investigate the structure of some vitreous and vitroceramics germanate systems obtained by melt and quenching method. Their characterization was performed both by well-known experimental spectroscopy techniques like: FT-IR, UV-VIS, EPR; X-ray diffraction and density measurements, as well as their structure was investigated using molecular modeling with the Gaussian program.

This work contains four chapters, as follows: i) the first chapter presents theoretical data related to the methods of preparation of glasses and some techniques of investigation; ii) the second chapter reviews some results obtained in the literature on systems that have in their matrix germanium dioxide; iii) the first part of chapter three describes several theoretical methods related to molecular modeling and in the second one are presented my own results obtained by molecular modeling of the structure of vitreous systems that contain germanium dioxide in their matrix; iv) the fourth chapter presents the experimental results obtained by investigating structural properties of eight vitreous and vitroceramics germanate systems doped with rare earth and transition metals. The conclusions I reached after performing the study of each system

appear immediately after each presentation and the final conclusions are listed at the end of the paper. The references are presented at the end of each chapter. In chapter four, I presented separately the references to my articles that constitute this thesis.

CHAPTER 1

METHODS FOR PREPARATION AND INVESTIGATION OF GLASSES

Oxide glasses are included into the category of non-crystalline solids. The term describes the class of non-crystalline solid material that although atoms are disposed at a similar distance that in crystalline solids, their arrangement in space is not regular. In a first approximation by glasses one can understand all crystalline solids, regardless of their chemical composition and the temperature stiffening, as a result of the gradual increase in viscosity, it's shows similar mechanical properties of solids, and this transition from liquid the vitreous state must be reversible. They are solid crystalline structure characterized by short distance sequence that shows the vitreous transition. Obtaining this structure by various methods must be repeated if they fully meet the same conditions for obtaining them [1].

In this chapter are presented the methods of preparation of glasses, and the first of them, that of melt and quenching, we used to prepare the systems investigated in this thesis. These systems are presented in the following table.

Also in this chapter are presented some of the methods of investigation of vitreous systems: UV-VIS, FT-IR, EPR spectroscopy, X-ray diffraction and density measurements, the methods that we used in analyzing the samples obtained.

Systemul oxidic vitros	Concentratia x%mol									
$x\text{CuO}\cdot(100-x)[7\text{GeO}_2\cdot 3\text{PbO}_2]$	0	1	5	10	-	20	30	40	-	60
$x\text{CuO}\cdot(100-x)[7\text{GeO}_2\cdot 3\text{PbO}_2\cdot 0.05\text{Al}_2\text{O}_3]$	0	1	5	10	-	20	30	-	-	-
$x\text{Fe}_2\text{O}_3\cdot(100-x)[7\text{GeO}_2\cdot 3\text{PbO}_2]$	0	1	5	10	15	20	30	40	50	60
$x\text{MoO}_3\cdot(100-x)[7\text{GeO}_2\cdot 3\text{PbO}_2]$	0	1	5	10	15	20	30	-	-	-
$x\text{WO}_3\cdot(100-x)[7\text{GeO}_2\cdot 3\text{PbO}_2]$	0	1	5	10	15	20	30	40	-	-
$x\text{Gd}_2\text{O}_3\cdot(100-x)[\text{TeO}_2\cdot \text{GeO}_2]$	0	-	5	10	15	20	-	40	50	-
$x\text{Gd}_2\text{O}_3\cdot(100-x)[\text{GeO}_2\cdot \text{V}_2\text{O}_5]$	0	1	5	10	15	20	-	-	-	-

CHAPTER 2

PRESENTATION OF SOME GERMANATE SYSTEMS STUDIED IN LITERATURE

In this chapter are presented some germanate systems studied in literature, which represents a small part of the realization of this thesis bibliography.

CHAPTER 3

THE COMPUTATIONAL MODELING OF VITREOUS SYSTEMS PROPERTIES

This chapter contains two important parts: the first one in which is described some theoretical aspects referred to Molecular Modeling and it's methods, and the second part contains some

experimental results obtained using the DFT method for some of study systems.

The connection between different methods used by molecular modeling is represented by the following diagram:

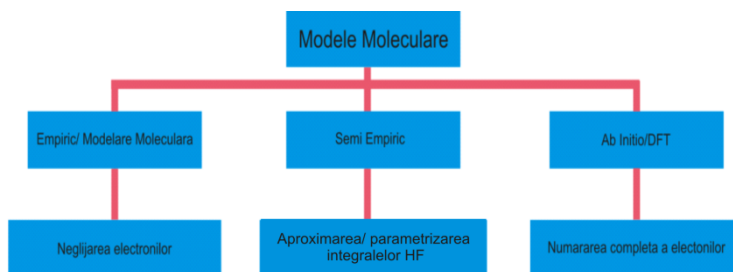


Fig. 3.1. The connection between different Molecular Models

The starting structures have been built using the graphical interface of Spartan'04 [2] and preoptimized by molecular mechanics. Optimizations were continued at DFT level (B3PW91/CEP-4G/ECP) using the Gaussian'03 package of programs [3].

3.3.1. Molecular modeling of $\text{GeO}_2 \cdot \text{V}_2\text{O}_5$

At first the structure of system $\text{GeO}_2 \cdot \text{V}_2\text{O}_5$ was modeled. The structural chemistry of crystalline oxides such as V_2O_5 revealed that the structure of V_2O_5 is built of octahedrons, where the pentavalent vanadium has five-coordination with oxygen atoms. The study on structural modifications of the vitreous network and the equilibrium geometry were found by optimization of octahedral $[\text{GeO}_6]$ structural units, it found that the Ge-O bonds are subdivided

into two groups: two bonds have shorter interatomic distance (1.875Å) and four bonds have longer interatomic distances (2x1.881 and 2x1.882Å).

The obtained data was used to calculate a possible structural model for the $\text{GeO}_2\cdot\text{V}_2\text{O}_5$ network. Similar methodology has previously been reported to study other glasses [5-8]. The study on structural modifications of the vitreous network and the equilibrium geometry were found by optimization of the structure presented in (Fig.3.3).

The distribution of the electronic states of the homo , homo^{-1} , lumo and lumo^{+1} can be seen in (Fig. 3.4). An interesting finding in these systems is that:

i) The homo and homo^{-1} give character of electron donor for the [VO4], [VO5] structural units of the vanadate glasses network and the [GeO6] structural units.

ii) The lumo and lumo^{+1} give the character of electron

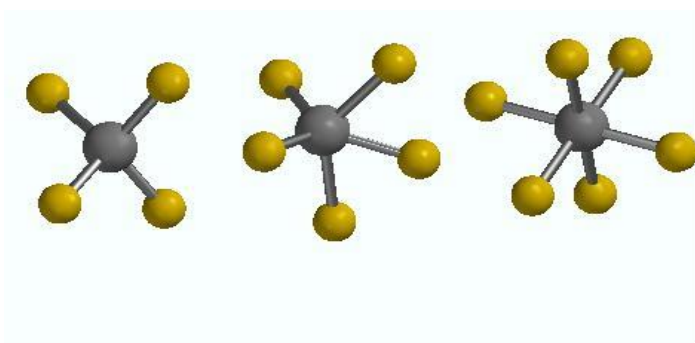


Fig. 3.2. The optimization structure for structural units a) [GeO₄], b) [GeO₅] si c) [GeO₆] [4].

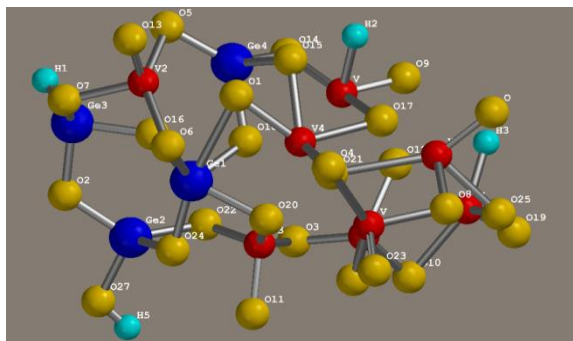


Fig. 3.3 The geometry optimization of the $\text{GeO}_2 \cdot \text{V}_2\text{O}_5$, [4] acceptor for the $[\text{GeO}_4]$ structural units of the germanate network and the $[\text{VO}_n]$ structural units of the vanadate network.

The massive vibrations of the $[\text{VO}_n]$ structural units can be coupled each other via $[\text{GeO}_6]$ and $[\text{GeO}_4]$ structural units. This leads to the splitting of the bridge modes and a multiplication of the number of these bands.

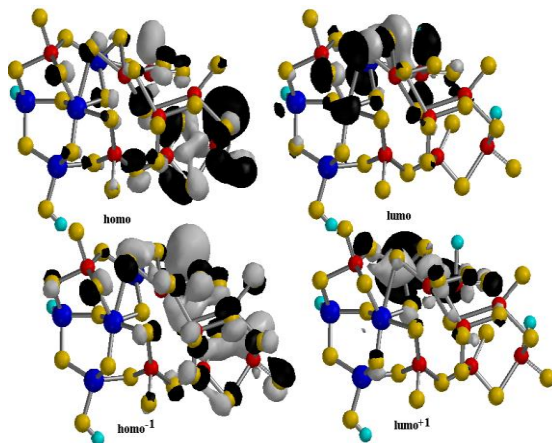


Fig.3.4 The distribution of the electronic states of the: homo, homo⁻¹, lumo, lumo⁺¹ of the proposed model for $\text{GeO}_2 \cdot \text{V}_2\text{O}_5$, [4]

3.3.2. Molecular modeling of $\text{CuO}\cdot[7\text{GeO}_2\cdot 3\text{PbO}_2]$

Lead germanate glasses can be fabricated as optical fibers and photosensitive waveguides for use in the field of optoelectronics and are excellent hosts for the development of luminescent devices. Lead oxide is unique in its influence on the structure of glasses. The study on structural modifications of the vitreous network and the equilibrium geometry were found by optimization of $\text{CuO}\cdot[7\text{GeO}_2\cdot 3\text{PbO}_2]$ (Fig. 3.5), there are some sites in our model, that are revealed in the thesis.

The observations present in these mechanisms show that the lead ions have an affinity pronounced towards structural units with non-bridging oxygens yielding the strong deformation of the $[\text{GeO}_6]$ structural units. Further the excess of oxygen can be accommodated in the host network by the formation of the $[\text{CuO}_n]$ entities. On the other hand, the formation of the $[\text{CuO}_4]^{-2}$ is a necessary for the compensation of charge of the Pb^{+2} ions.

The distribution of the electronic states of the HOMO and LUMO can be seen in (Fig. 3.6). An interesting finding in these systems is that:

- i) The HOMO gives character of electron donor for the $[\text{PbO}_3]$, $[\text{GeO}_4]$ and $[\text{CuO}_n]$ structural units.
- ii) The LUMO gives the character of electron acceptor for the $[\text{GeO}_4]$ and $[\text{PbO}_4]$ structural units of the network.

There is a charge transfer between the lead atoms tri- and tetra-coordinated. This can be explained considering that the lead-germanate network is flexible to form the appropriate coordination

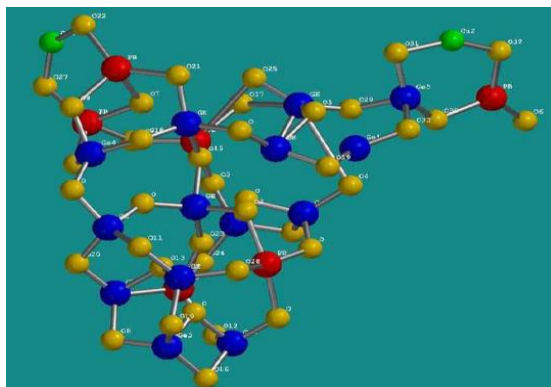


Fig. 3.5 The geometry optimization of the $\text{CuO}\cdot[7\text{GeO}_2\cdot 3\text{PbO}_2]$

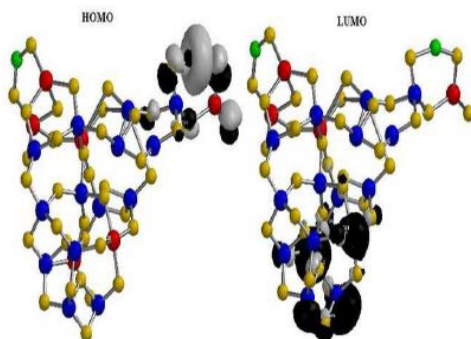


Fig. 3.6 The distribution of the electronic states of the: HOMO and LUMO of the proposed model for $\text{CuO}\cdot[7\text{GeO}_2\cdot 3\text{PbO}_2]$

environments with structural units of opposite charge such as copper ions, $[\text{CuO}_4]^{2-}$.

3.3.3 Molecular modeling of 20MoO₃·80[7GeO₂·3PbO]

MoO₃ is a transition metal oxide, belonging to the intermediate class of glass forming oxides which may participate in the glass network forming in the presence of modifier oxides like PbO, but it may also act as a modifier [9]. Moreover, glasses containing molybdenum ions have interesting optical and electrical properties depending on the type and composition of glass and the different valence states of molybdenum ions [10]. Such peculiar properties are related to the ability of molybdenum ions to exist in glasses in four possible valences, namely Mo³⁺, Mo⁴⁺, Mo⁵⁺ and Mo⁶⁺ [11-13].

The process of doping the host network with molybdenum ions causes changes in the intensity of some FTIR bands but the main characteristic IR features keep their position. These changes in the intensities of the IR bands are related to the possible variations in the bond length and bond angles of the vibrating structural units. In this view, quantum chemical calculations will be used in order to understand the local structure of the 20MoO₃·80[7GeO₂·3PbO] glass network. Similar methodology has previously been reported to study other tellurate glasses [5-7].

The structural model obtained for the 20MoO₃·80[7GeO₂·3PbO] glass and shown in (Fig. 3.7) gives detailed information concerning the Ge-O, Pb-O framework structure and the environment of molybdenum ions.

The model indicates that there is very small number of [GeO₆] structural units and these have a deformed octahedral

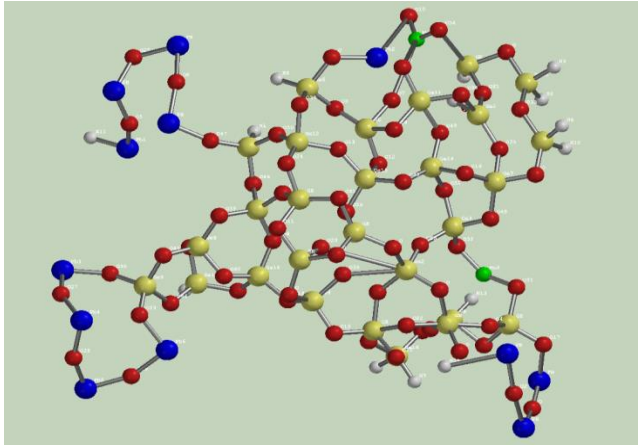


Fig. 3.7 The geometry optimization of the $20\text{MoO}_3 \cdot 80[7\text{GeO}_2 \cdot 3\text{PbO}]$

geometry. The Ge-O bond length increases its equilibrium value from $1.78\text{-}1.81\text{\AA}$ to over 2.61\AA (two Ge-O interatomic distances) equivalent to breaking these bonds. There is instability between the nonequivalent Ge-O bonds in the octahedron and at tridimensional level the tetragonal $[\text{GeO}_4]$ structural units becomes favorite.

3.3.4 Molecular modeling of $20\text{WO}_3 \cdot 80[7\text{GeO}_2 \cdot 3\text{PbO}]$

It is well known that the electrical properties of vitreous/crystalline materials depend on their structures. The structural units of the glass former may play a major role in deciding the nature of the conduction in the glass matrices. For example, tungsten in glasses might coexist in different valence states, mainly W^{+5} and W^{+6} , depending on host glass composition and preparation conditions and an electron transfer between tungsten cations is

permitted. The semiconducting properties of glasses are due to such electron transfer [15].

Our results show that the process of doping the host network with tungsten ions causes changes in bond length, bond angles of the vibrating structural units and an expansion of the structure for relaxation and accommodation of the glass network with the excess of oxygen. In this view, quantum chemical calculations will be used in order to understand the local structure of the $20\text{WO}_3 \cdot 80[7\text{GeO}_2 \cdot 3\text{PbO}]$ glass network.

The optimized geometry of the structural model proposed for $20\text{WO}_3 \cdot 80[7\text{GeO}_2 \cdot 3\text{PbO}]$ glass network is shown in (Fig. 3.8). The detailed information concerning the Ge-O, Pb-O, W-O bond lengths of framework structure indicate the nonequivalent Ge-O bonds in the $[\text{GeO}_6]$ and $[\text{GeO}_4]$ structural units.

The distribution of the electronic states of the *homo* and *lumo* can be seen in (Fig. 3.9). An interesting finding in these systems is that: i) the *homo* and *homo*⁻¹ give character of electron donor for the $[\text{GeO}_4]$, $[\text{WO}_n]$ and $[\text{PbO}_4]$ structural units; ii) the *lumo* and *lumo*⁺¹ give the character of electron acceptor for the $[\text{PbO}_n]$ structural units of the network.

This charge transfer can be explained considering that the lead ions are flexible to form the appropriate coordination environments with structural units of opposite electric charge such as $[\text{WO}_4]$ and $[\text{GeO}_4]$.

In brief, we assume that the lead and germanium atoms do not accommodate with the non-bridging oxygens and the excess of

the oxygen ions. The accommodation of the network is possible by increase of $[\text{WO}_n]$ polyhedrons and the formation of PbWO_4 crystalline phase, in agreement with XRD data.

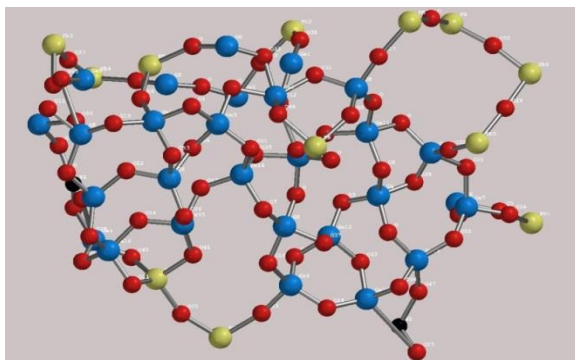


Fig. 3.8 The geometry optimization of the $20\text{WO}_3 \cdot 80[7\text{GeO}_2 \cdot 3\text{PbO}]$ glass network

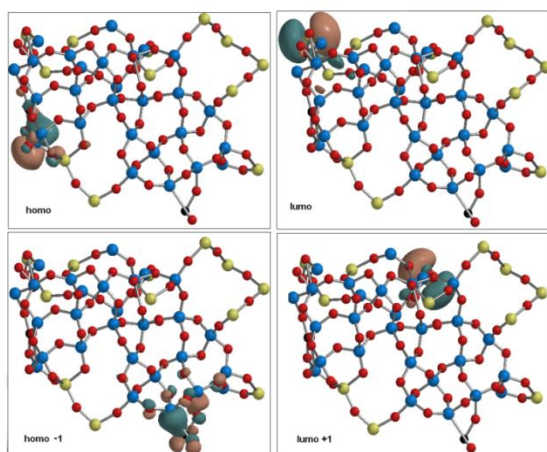


Fig. 3.9 The distribution of the electronic states of the: homo, homo⁻¹, lumo, lumo⁺¹ of the proposed model for $20\text{WO}_3 \cdot 80[7\text{GeO}_2 \cdot 3\text{PbO}]$ glasses.

CAPITOLUL 4

PERPARATION AND STRUCTURAL CHARACTERIZATION OF SOME GERMANATE GLASSES SYSTEMS

In this chapter there are shown the spectroscopy EPR, FT-IR and UV-VIS studies, as well as density measurement and X-ray diffraction patents due to the investigation systems in order to determinate their structure and possible practical applications of the obtained glasses. Thus we investigated a set of eight germanate systems; which were each doped with metal oxides and / or rare earth oxides.

The equipment used for analyzing the samples was as follows:

- For X-ray diffraction we used a XRD-6000 Shimadzu diffractometer, with a monochromator of graphite for the Cu-K α radiation ($\lambda=1.54\text{\AA}$) at room temperature.
- For FT-IR measurements we used a JASCO FTIR 6200 spectrometer using the using the KBr pellet technique.
- For UV-VIS: a Perkin-Elmer Lambda 45 spectrometer.
- EPR measurements were performed at room temperature using ADANI Portable EPR PS 8400-type spectrometer, in X frequency band (9.1GHz) and a field modulation of 100kHz. The microwave power used was 5mW.
- For density measurements: the pycnometer method was used

4.2 Structural studies of $x\text{CuO}\cdot(100 - x)[7\text{GeO}_2\cdot 3\text{PbO}_2]$

The X-ray diffraction patterns did not reveal the crystalline phase in the samples up to 60% mol CuO.

4.2.1. FT-IR spectroscopy measurements

Presence of multiple cations of germanium, lead and copper in the glasses to attract the oxygen atoms for compensation of charge yield a competition between these cations. This preference is decided by the electronegativity. The covalency of Pb-O are stronger than Ge-O and Cu-O, respectively. As a result, the higher affinity of the lead ions to attract oxygen atoms yields the apparition of $[\text{PbO}_n]$ ($n=3, 4$) structural units.

4.2.2 UV-VIS spectroscopy measurements

In glasses, copper ions exist in two stable ionic states, monovalent Cu^{+1} ions, divalent Cu^{+2} ions and may also exist as metallic copper. It follows from the spectrum that the glass matrix absorption begins at about 250nm. The examinations of these spectra show that by increasing of the CuO content the characteristic UV-VIS bands are modified.

New bands appear in the 250-260 nm region and at about 270nm. These peaks may be ascribed to $3d^{10} \rightarrow 3d^9 4s^1$ transition; these transitions are forbidden transitions, but in this case they may occur due to low symmetry of local electric field around Cu^{+1} ions [16, 17]. The highest intensity of these peaks observed in the spectrum of glass with $x=40\%$ mol CuO suggests the presence of

larger concentration of Cu^{+1} ions in this glass. Such reduction indicates the conversion of a part of Cu^{+2} ions into Cu^{+1} ions while the Pb^{+2} ions undergo to Pb^{+4} ions.

The instability of the $[\text{GeO}_6]$ structural units yields the formation of the $[\text{O}=\text{GeO}_4]$ structural units. The $[\text{GeO}_5]$ structural units will yield new electronic transitions attributed to the O=Ge bond in the UV-VIS spectra. For sample with $x=20$ and 40% mol CuO these structural units attain maximum value.

4.2.3 Density measurements

(Fig. 4.2) shows the compositional evolution of the density of copper-lead-germanate glasses. It is observed that transition metal ion acts as a network modifier because this dependence is not linear suggesting the occurrence of structural changes of the host vitreous

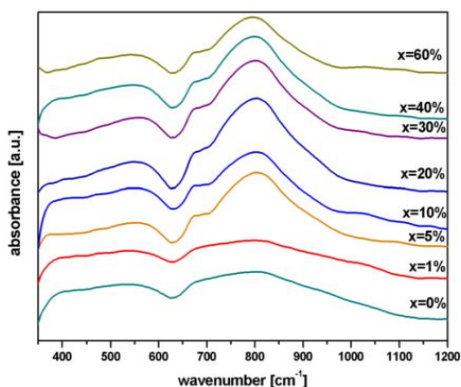


Fig.4.1 FT-IR spectra of $x\text{CuO} \cdot (100-x)[7\text{GeO}_2 \cdot 3\text{PbO}_2]$ glasses.

matrix.

4.2.4. EPR spectroscopy measurements

Copper has the electronic configuration $[\text{Kr}] 4d^{10} 5s^1$. Apparently, Cu^{+1} and Cu^{+2} ions are the major valence state of copper in the glasses under study. The Cu^{+1} ions with the $4d^{10}$ configuration give no EPR spectra. The Cu^{+2} ion, with $S=1/2$, has a nuclear spin $I=3/2$ for both ^{63}Cu and ^{65}Cu . In the present work, four parallel hyperfine components are observed. The values of $g_{\parallel}=2.33$ and $g_{\perp}=2.03$ suggest that the Cu^{+2} ions in the glasses are

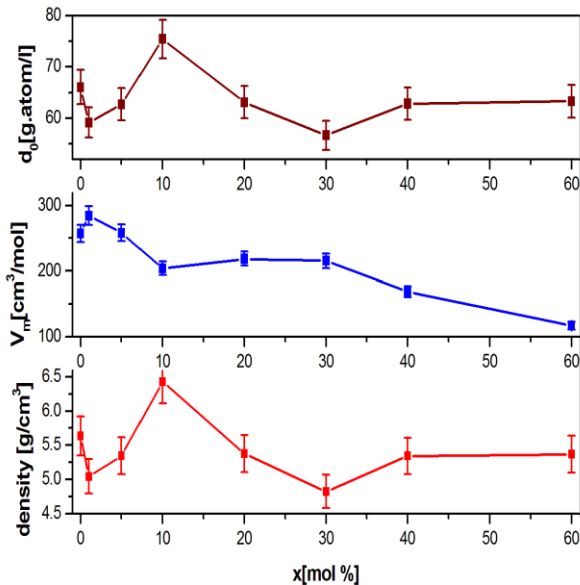


Fig.4.2 Dependence on a) density, b) molar volume, V_m and c) the oxygen packing density, d_o

coordinated by six ligands that form an octahedron elongated along the z-axis [17]. The value $g_{\parallel} > g_{\perp} > g_e$ ($g_e = 2.002$) shows that the ground state of Cu^{+2} ions is $d_{x^2-y^2}$ orbital (${}^2B_{1g}$ state).

4.3. Structural studies of $x\text{CuO} \cdot (100-x)[7\text{GeO}_2 \cdot 3\text{PbO}_2 \cdot 0.05\text{Al}_2\text{O}_3]$

Adding Al_2O_3 to lead-germanate vitreous systems remains a topic of interest because there is not a clear model of how oxygen polyhedra surrounding metal atoms, the role it plays the other elements of glass or the tendency for nonspecific vitreous systems.

4.3.1. FT-IR spectroscopy measurements

FTIR spectra obtained for vitreous system with the following composition $x\text{CuO} \cdot (100-x)[7\text{GeO}_2 \cdot 3\text{PbO}_2 \cdot 0.05\text{Al}_2\text{O}_3]$ where $x = 0, 1, 5, 10, 20$ and 30 %mol CuO are shown in (Fig. 4.3). Spectrum contains stretching vibrations due to Ge-O, Pb-O and Al-O bonds of different structural units. Thus, the intense band located at $\sim 820 \text{ cm}^{-1}$ is attributed to deformation vibrations of Ge-O-Ge bonds in $[\text{GeO}_4]$ tetrahedral structural units [18-22]. Band located at about 700 cm^{-1} corresponds to vibrations of the Ge-O bonds in the $[\text{GeO}_6]$ structural units [23-25].

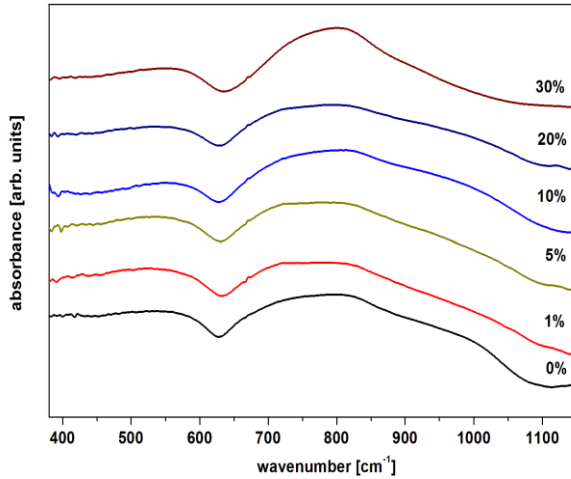


Fig. 4.3 FT-IR spectra of $x\text{CuO}\cdot(100-x)[7\text{GeO}_2\cdot 3\text{PbO}_2\cdot 0.05\text{Al}_2\text{O}_3]$ glasses.

4.3.2. UV-VIS spectroscopy measurements

UV-VIS absorption spectrum of the host matrix begins with a rising absorption band situated at about 250 nm. This band can be assigned to the Ge-O-Ge wrong bonds [26].

The changes in amplitude and bandwidth of the UV-VIS features are drastically modified depend on the content of CuO. For sample with $x=5$ %mol CuO, the number of the Ge^{+2} centers attains minimum value indicating that the content of $[\text{GeO}_6]$ structural units became maximum. The band situated at about 300 nm corresponds

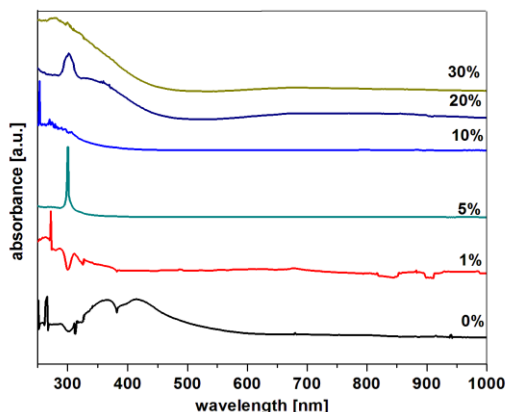


Fig 4.4 UV-VIS absorption spectra of $x\text{CuO}-(100-x)[7\text{GeO}_2\cdot 3\text{PbO}_2\cdot 0.05\text{Al}_2\text{O}_3]$ glasses.

to the Cu^{+2} and Pb^{+2} ions [27]. The intensity of this band increases by increasing of CuO content up to 30% mol.

4.3.3 EPR spectroscopy measurements

In this paper we discuss some EPR data in order to obtain more information about the local structure and the interactions between the copper ions in glasses. The EPR spectra of CuO substituted quaternary glasses, are characterized by a broad resonance line around at $g\sim 2$. The line width increases as copper concentration increases.

The ESR spectra of the samples with $x=1$ % CuO show only line narrowing but do not show any resolved hyperfine splitting. The absence of hyperfine structure can be assigned to formation of $\text{Cu}^{+2}\text{-Ge}^{+4}$ (or $\text{Cu}^{+2}\text{-Ge}^{+2}$) exchange pairs which are weakly coupled

though the oxygen atom. The line at $g \sim 2$ is not seen clearly in samples with $x \geq 20$ % mol CuO because of increased line broadening.

4.4 Structural studies of $x\text{Fe}_2\text{O}_3 \cdot (100 - x)[7\text{GeO}_2 \cdot 3\text{PbO}]$

Lead-germanate glasses show interesting optical properties and it is expected that the introduction of an iron oxide component into the binary lead-germanate glasses may affect the structural features of the host matrix. In the present work iron-lead-germanate glasses were studied in order to understand the structural mechanism responsible for the germanate anomaly.

4.4.1 X-ray diffraction measurements

The X-ray diffraction patterns did not reveal any crystallinity in the samples with $x < 60$ % mol Fe_2O_3 . However, at the composition $x = 60$ % mol Fe_2O_3 Bragg peaks associated with the

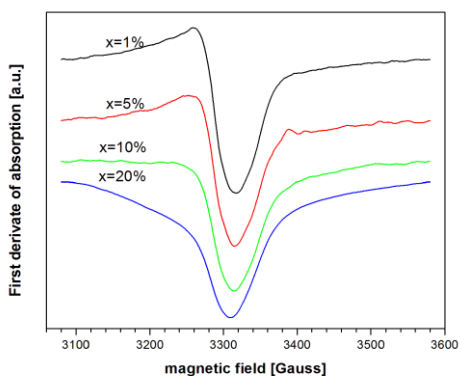


Fig. 4.5 EPR spectra of $x\text{CuO} \cdot (100-x)[7\text{GeO}_2 \cdot 3\text{PbO}_2 \cdot 0.05\text{Al}_2\text{O}_3]$ glasses.

Fe₂O₃ crystalline phase were observed (Fig.4.8).

4.4.2 FT-IR spectroscopy measurements

The increase of Fe₂O₃ content up to 60%mol results in the conversion of some [FeO₄] to [FeO₆] structural units [28]. This is indicated by a new band situated at about 470cm⁻¹, which is associated with vibrations of the Fe-O bond from [FeO₆] structural units. A noticeable change appears also in the characteristic features of the [GeO₄] structural units (band located at about 788cm⁻¹). These modifications explain the conversion of some [GeO₆] to [GeO₄] structural units while the [FeO₄] structural units are transformed to the [FeO₆] structural units. On the other hand, a growth followed by a decline of the number of [GeO₆] octahedral structural units in the glass network constitutes the germanate anomaly. The currently accepted model for this mechanism is a change of the coordination of the germanium from 4-coordinated to higher coordinated species such as [GeO_n] structural units where n=5 and 6.

In brief, the lead ions are a unique influence on the structure of the iron-lead-germanate glasses. The lead atoms which form covalent bonds participate as network former, while the lead ions which form ionic bonds have a strong affinity towards [GeO₅] and [FeO₄] structural units containing non-bridging oxygens.

4.4.3 UV-VIS spectroscopy measurements

For all glasses, the UV absorption bands begin at 250nm by an ascending lobe. These UV absorption bands are assumed to originate

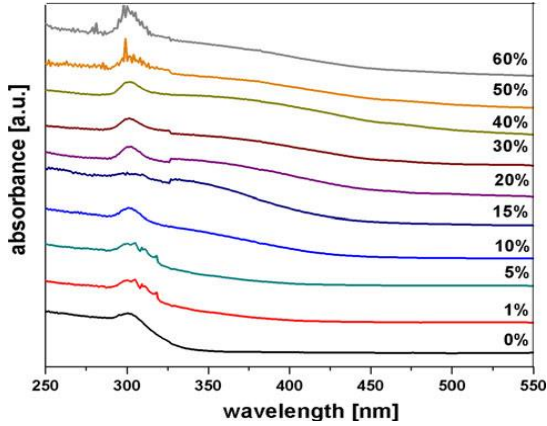


Fig. 4.6 UV-VIS absorption spectra of $x\text{Fe}_2\text{O}_3 (100-x)[7\text{GeO}_2 3\text{PbO}]$ glasses.

from lead germanate host matrix. The stronger transitions in the UV-VIS spectrum can be due to the presence of the Ge=O bonds from $[\text{GeO}_5]$ structural units and Pb=O bonds from $[\text{PbO}_3]$ structural units which allow $n-\pi^*$ transitions.

For samples containing $x \geq 50\text{mol } \%$ Fe_2O_3 , the apparition of new bands located in the 260-325nm region is correlated to the possible distortion of the iron species symmetry, the presence of the larger number of Pb^{+2} ions and the apparition of the new iron species derived from the Fe_2O_3 crystalline phase, in agreement with the XRD data.

4.5 Structural study of ternary iron-lead-germanate glass ceramics

In the present work, the devitrification behavior of the iron-lead-germanate glasses was studied by X-ray diffraction, Fourier-

transform infrared spectroscopy (FTIR) and ultraviolet-visible spectroscopy (UV-VIS).

4.5.1 X-ray diffraction measurements

The X-ray diffraction analysis reveals crystalline phases in the heat-treated samples at 400⁰C for 8h.. By increasing of the iron (III) oxide content up to 10%mol, X-ray diffraction patterns show three α -PbGe₄O₉, γ -PbGe₄O₉ and PbO_{1.44} crystalline phases. At the composition x=60%mol Fe₂O₃, Bragg peaks associated with the pure Pb₃Fe₂Ge₄O₁₄ crystalline phase were observed.

4.5.2 FT-IR spectroscopy measurements

The FT-IR spectroscopy data suggest that with increasing the amount of Fe₂O₃ in the vitreous matrix the number of [GeO₆], [PbO₆] and [FeO₆] structural units increases.

4.5.3 UV-VIS spectroscopy measurements

UV-VIS spectra show that with increasing of Fe₂O₃ content, network continuity breaks down with the formation of larger numbers of non-bridging oxygens.

4.6. Structural studies of xMoO₃ (100-x)[7GeO₂ 3PbO]

MoO₃ is a transition metal oxide, belonging to the intermediate class of glass forming oxides which may participate in the glass network forming in the presence of modifier oxides like PbO, but it may also act as a modifier [9].

4.6.1. X-ray diffraction measurements

The X-ray diffraction patterns did not reveal any crystalline phase in the samples with $x < 20\%$ mol MoO_3 . Then, in the sample with $x = 25\%$ mol MoO_3 , the presence of the GeO_2 crystalline phase (tetragonal system) was detected. By increasing of the MoO_3 content up to 30% mol, X-ray diffraction patterns show the apparition of GeO_2 and PbMoO_4 crystalline phases.

4.6.2 Density measurements

A simple inspection of the density, molar volume (V_m) and oxygen packing density (d_o) data suggests that the gradual addition of molybdenum ions generates changes of the basic structural units of the glass matrix. The increasing of the molybdenum content of the samples determines an almost linear decrease of the molar volume. This decrease is associated with a decrease in the number of non-bridging oxygens and with a contracting effect of the network due to the formation of $[\text{GeO}_6]$ structural units which are slightly larger in size than the $[\text{GeO}_4]$ species.

4.6.3 FT-IR spectroscopy measurements

The structure of the base glass is characterized by a large number of non-bridging oxygens and therefore is relatively open. The observations presented above show that by increasing the MoO_3 content of samples up to 10% mol, the $[\text{GeO}_4]$ tetrahedral structural units were converted in $[\text{GeO}_6]$ octahedral structural units up to a maximum. In this manner the excess oxygen added to the glass by

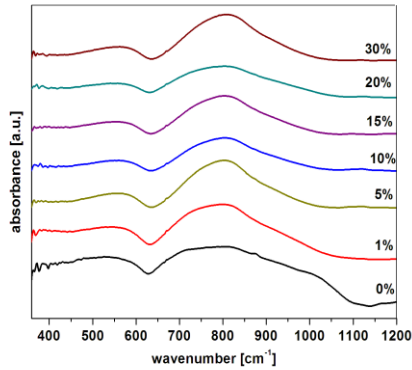


Fig. 4.7 FT-IR absorption spectra of $x\text{MoO}_3 \cdot (100-x)[7\text{GeO}_2 \cdot 3\text{PbO}]$ glasses.

the addition of MoO_3 is taken up by forming isolated $[\text{GeO}_6]$ octahedral structural units. The pronounced affinity towards molybdate anions yields the formation of the PbMoO_4 crystalline phase

4.6.4 UV-VIS spectroscopy measurements

Figure 4.8 shows the UV-VIS spectra of molybdenum-lead-germanate glasses and glass ceramics containing different concentrations of MoO_3 . With increasing concentration of molybdenum ions there is a gradual increase in the intensity of these bands, attaining a maximum for the sample with $x = 20\%$ mol MoO_3 . With the addition of MoO_3 to the host network, the absorption edge is found to be shifted gradually towards higher wavelength side.

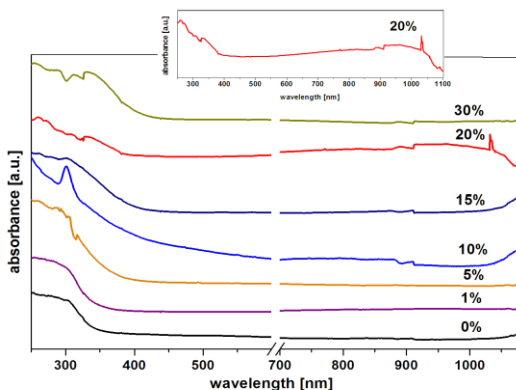


Fig. 4.8 UV-VIS absorption spectra of $x\text{MoO}_3 \cdot (100-x)[7\text{GeO}_2 \cdot 3\text{PbO}]$ glasses.

4.6.5 EPR spectroscopy measurements

The shape of the EPR spectra was observed to vary by increasing the MoO_3 content of the samples. For all the studied glasses, the EPR spectra revealed the existence of a signal centered near $g \sim 5.2$. This signal is associated with the presence of Mo^{+3} ions [30, 31].

4.7 Structural studies of $x\text{WO}_3 \cdot (100-x)[7\text{GeO}_2 \cdot 3\text{PbO}]$

The aim of this work is to investigate the effect of WO_3 on the structural, optic and electronic properties of $x\text{WO}_3 \cdot (100-x)[7\text{GeO}_2 \cdot 3\text{PbO}]$, with $x = 0 - 40\%$ mol glasses and glass ceramics in the view of applications at electrochemical devices.

4.7.1 X-ray diffraction measurements

X-ray diffraction patterns of different compositions of the prepared samples are shown in (Fig. 4.9). In the samples with $x \leq 30\%$ mol WO_3 , X-ray diffraction patterns exhibit broader halos, characteristic of the amorphous materials. Then, in the sample with $x = 40\%$ mol WO_3 , the presence of the PbWO_4 crystalline phase was detected.

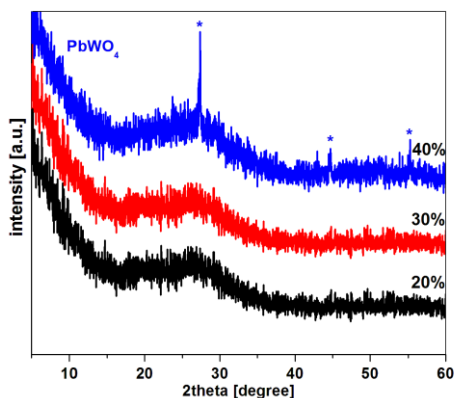


Fig. 4.9 XRD diffraction patterns of the $\text{WO}_3 \cdot (100-x)[7\text{GeO}_2 \cdot 3\text{PbO}]$ glasses.

4.7.2 FT-IR spectroscopy measurements

A simple inspection of the FTIR spectra suggests that the WO_3 incorporation yields network distortions that can be monitored by the progressive broadening of the bands centered at about 470, 520 and 800cm^{-1} . On the other hand, experimental FTIR spectra indicate that tungsten-lead-germanate glasses containing dopant up

to 40% level, reveal the general maintenance of the main characteristic network structural units and also show important features reflecting the depolymerizing effect of WO_3 addition on the lead-germanate network.

4.7.3 UV-VIS spectroscopy measurements

The studied glasses and vitroceraamics containing up to higher WO_3 concentrations reveal high electronic transitions absorption consisting of two successive sharp bands situated between 250 and 360nm and followed by a broad unsymmetrical visible band centered at about 700nm. The intensities of UV-VIS absorption bands increase with the addition of WO_3 dopant and accordingly and their interpretation is summarized in my thesis.

The optical absorption spectra exhibit consisting of

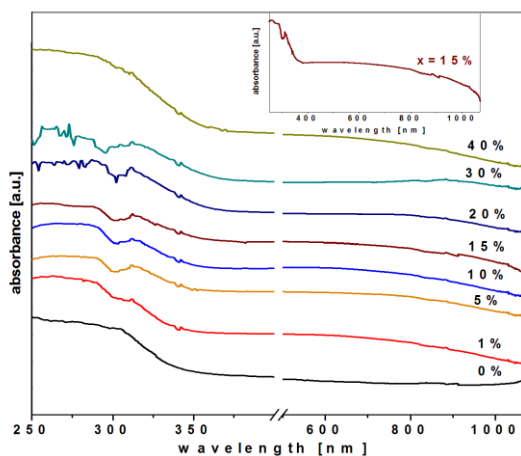


Fig. 4.10 UV-VIS absorption spectra of $x\text{WO}_3 \cdot (100-x)[7\text{GeO}_2 \cdot 3\text{PbO}]$ glasses.

successive sharp bands situated in the ultraviolet and visible domain and show the existence of $[\text{PbO}_3]$ structural units, $[\text{WO}_4]$ structural units, Pb^{+2} and W^{+5} ions in the tungsten-lead-germanate glasses and vitroceramics. From this observation it is concluded gradual transformation of the tungsten ions from tetrahedral to octahedral positions and increasing modifying action of tungsten ions in the glass and vitroceramics network and with increase in the WO_3 concentration.

4.7.4 EPR spectroscopy measurements

The spectra of these systems exhibit a hyperfine structure with an asymmetric signal situated at about $g_{\perp}=1.7$ and $g_{\parallel}=1.6$, characteristic of W^{+5} ions (nd^1 electronic configuration) having a C_{4v} local symmetry in oxide glasses [32,33]. This signal indicates that W^{+5} ions present in axially distorted octahedral positions with a short W-O bond and an opposite long W-O bond along the symmetry axis of oxygen ions [34].

The shapes of the EPR spectra depend on the WO_3 content in glasses. The signal intensity is approximately invariant, the amount of W^{+5} centers remains constant and the values of g remain unaffected when the WO_3 concentration is ranged between $x \leq 5$ and $x \geq 30\% \text{ molWO}_3$.

4.8. Structural studies of $x\text{Gd}_2\text{O}_3 \cdot (100-x)[\text{TeO}_2 \cdot \text{GeO}_2]$

Germanate glasses doped with rare earth ions were investigated extensively in the past because their physicochemical,

optical and spectroscopic properties are advantageous for optoelectronic applications. Tellurium oxide is a heavy metal oxide, and when it is introduced in the glass matrix, it may influence the physical properties as refractive index, thermal expansion coefficient, chemical resistance, infrared transmittance of the glasses and further makes the glasses suitable for use as devices for communication and advanced computer applications. When doped with a different kind of rare earth ions, these glasses find wide use in high power laser technology, sensor, optical switching and amplifiers for fibre communications.

There were studied the vitreous materials of the system $x\text{Gd}_2\text{O}_3 \cdot (100-x)[\text{TeO}_2 \cdot \text{GeO}_2]$ where $x = 0\text{--}50\%$ mol.

4.8.1 FT-IR spectroscopy measurements

By increasing the Gd_2O_3 content up to 10%mol, the evolution of the structure can be explained considering the accommodation of the network with excess of oxygen by the formation of $[\text{GeO}_6]$ structural units. Then by the increasing of Gd_2O_3 content up to 20%mol a sharp of decreasing trend was observed in intensity of the band situated in the 700cm^{-1} region and new increasing trends towards larger wavenumber were exposed on the bands centered in the $800\text{--}950\text{cm}^{-1}$ region. Structural changes, as recognized by analyzing band shapes of FTIR spectra, revealed that Gd_2O_3 causes a change from the continuous germanium-tellurate network to the continuous germanate-tellurate network with interconnected through Ge-O-Ge, Te-O-Te and Ge-O-Te bridges.

The currently accepted model for this mechanism is a change of germanium from 4-coordinated to higher coordinated species ($x \leq 10\%$ mol) after that the number of [GeO6] structural units decreases ($10 < x \leq 20\%$ mol). This structural mechanism is responsible for the germanate anomaly with remains area of interest to the glass science [35, 36].

4.8.2 UV-VIS spectroscopy measurements

Incorporation of germanium ions in the glass was allowed photosensitivity effects with applications in the telecommunications, lasers and sensors. Photosensitivity has been explained by two mechanisms [37]: i) the formation of new paramagnetic defects after UV laser irradiation, depending on glass composition; ii) the densification of the glasses which can be correlated by the increase

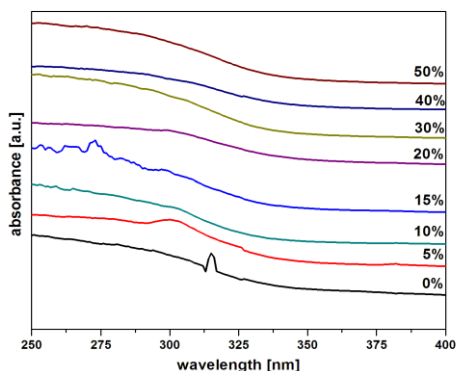


Fig. 4.11 UV-VIS absorption spectra of $x\text{Gd}_2\text{O}_3 \cdot (100-x)[\text{TeO}_2 \cdot \text{GeO}_2]$ glasses.

of refractive index. The term of densification of the glass implies a change in coordination of Ge^{+4} ions from 4-fold to 6-fold which will lead to glass compaction and then to refractive index increase.

The O=Ge bond of $[\text{GeO}_5]$ structural units show strong absorption in the ultraviolet due to allowed $n-\pi^*$ transition. The $[\text{GeO}_5]$ structural units are more stable thermodynamically than their analogues and the $[\text{GeO}_6]$ structural units produce the improvement of the amorphous character of these glasses.

4.8.3. EPR spectroscopy measurements

The Gd^{+3} ions doped germanate-tellurate glasses exhibit six resonance signals at $g \approx 2.0, 2.8, 3.3, 4.3, 4.8$ and 6 .

The Gd^{+3} ions in these glasses can be considered as isolated in the sense of the absence of clustering. The weakening intensity of the clusters EPR line could be due to the Gd^{+3} migrations inside the glass network. It should lead to the appearance of more Gd^{+3} content in network former positions. It can be pointed that the Gd^{+3} ions are generally suspected to improve their environment.

4.9 Studiul structurii sistemului $x\text{Gd}_2\text{O}_3 \cdot (100-x)[\text{GeO}_2 \cdot \text{V}_2\text{O}_5]$

4.9.1. Density measurements

This figure shows the presence of density maxima at $x=5$ and 20%mol Gd_2O_3 . The changes in molar volume, it appeared to be minimal at $x=5$ and 20%mol. We conclude that with increasing of the Gd_2O_3 content up to 5%mol, the local vanadium environment in

the glass changes from tetrahedral to pentagonal geometry due the fact that the coordination number of vanadium atoms changes from 4 to 5. Further the addition of the modifier gadolinium oxide to the vanadium germanate glass network introduces a surplus oxygen into the vitreous network and the need to accommodate of the glasses network. The additional oxygen may be incorporated into the network as non-bridging oxygen by breaking oxygen bridges and in these conditions the four-coordinated germanium atoms attain maximum value.

For $x \leq 5\% \text{mol}$ and $x = 20\% \text{mol}$ the oxygen packing density increases which clearly indicates that the glassy network becomes tightly packed when more Gd_2O_3 is introduced to the vitreous matrix.

4.9.2. FT-IR spectroscopy measurements

Analyzing the structural changes resulted from the IR spectra, we found that the gadolinium ions have a pronounced affinity towards $[\text{VO}_4]$ structural units which contain non-bridging oxygens necessary for the charge compensation. The introduction of the excess of oxygen yields the formation of $[\text{VO}_5]$ structural units. This attains maximum value at $5\% \text{mol Gd}_2\text{O}_3$, in agreement with the density measurements. Further, the addition of the surplus of oxygen implies the transformation of $[\text{VO}_5]$ to $[\text{VO}_4]$ structural units and the formation of VO_4^{3-} orthovanadate structural units. The formation of free orthovanadate units creates smaller network cavities, the increase of local densification and density (for sample with $x = 20\% \text{mol}$).

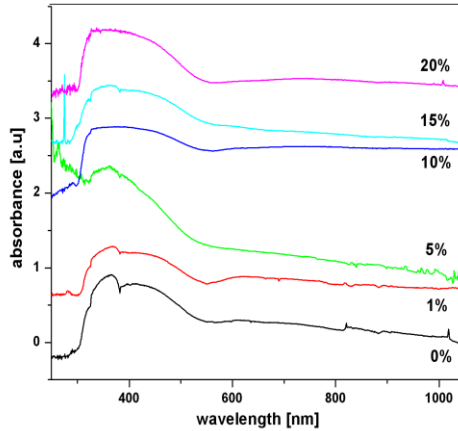


Fig.4.13 UV-VIS absorption spectra of $x\text{Gd}_2\text{O}_3 \cdot (100-x)[\text{GeO}_2 \cdot \text{V}_2\text{O}_5]$ glasses.

4.9.3. UV-VIS spectroscopy measurements

It follows from the spectrum that all the glasses samples show a strong absorption extending from about 300 to 530nm. This broad UV absorption is assumed to originate from the combination of vanadium ions possibly present in the three valences 3+, 4+ and 5+. Trivalent vanadium ions exhibit a characteristic UV band at 350-400nm, vanadyl tetravalent ions possess an absorption at about 420nm and pentavalent ions are known to belong to d^0 configuration and exhibit only UV bands.

The bands located at about 360nm correspond to the V^{+5} ions. These results show that the incorporation of Gd^{+3} ions in the host matrix have a directly influenced of $\text{V}=\text{O}$ bonds. The $\text{V}=\text{O}$

bonds are not conserved. The UV-VIS spectrum is dominated by the charge transfer of the type $O^{2-} \rightarrow V^{+5}$ [38, 39].

Selective conclusions

1. I prepared eight vitreous and vitroc ceramic systems doped with rare earth ions and transition metals using the melt and quenching method.
2. These systems were investigated by: i) FT-IR, UV-VIS and EPR spectroscopy ii) density measurements and iii) X-ray diffraction; the data obtained through these diverse measurements are in full agreement with each other.
3. The structural characteristics obtained experimentally for some of these systems were validated through molecular modeling simulations.
4. In the investigated systems so-called germanate anomaly was observed, which has been emphasized by both IR and UV-VIS spectroscopy measurements and molecular modeling via numerical simulations of their structure.
5. Moreover, for the system $x\text{CuO} \cdot (100 - x)[7\text{GeO}_2 \cdot 3\text{PbO}_2]$, it was studied the influence of Al_2O_3 addition on the properties of the matrix. The most important change is observed in the EPR spectra recorded for these systems, and is manifested by the disappearance of hyperfine structure in samples containing aluminum ions due to dipolar and super-exchange interactions, forming pairs like $\text{Cu}^{2+}\text{-O-Cu}^{2+}$.

Selective bibliography:

1. I.Ardelean, Introducere in studiul materialelor oxidice cu structura vitroasa, Ed.Nap.Star, Cluj-Napoca, 2002
2. Spartan'04, Wavefunction Inc., 18401 Von Karman Avenue, Suite 370 Irvine, CA 92612.
3. M. J. Frisch, et all, Gaussian 03, Revision A.1, Gaussian, Inc., Pittsburgh PA, 2003.
4. S. Rada, R. Chelcea, E. Culea, J Mol Model (2011) 17:165–171
5. S. Rada, M. Culea, E. Culea, J. Phys. Chem. A 112(44) (2008) 11251.
6. S. Rada, M. Culea, M. Neumann, E. Culea, Chem. Phys. Lett. 460 (2008) 196.
7. S. Rada, E. Culea, J. Molec. Struct 929 (2009) 141.
8. S. Rada, T. Ristoiu, M. Rada, I. Coroiu, V. Maties, E. Culea, Mater. Res. Bull. 45 (2010) 69.
9. I. Kashif, Samy A. Rahman, A.G. Mostafa, E.M. Ibrahim, A.M. Sanad, J. Alloys Compd. 450(1–2) (2008) 352-358.
10. M.A. Ghauri, S.A. Siddiqi, W.A. Shah, M.G.B. Ashiq, M. Iqbal, J. Non-Cryst. Solids, 355(50–51) 2009 2466-2471.
11. L. Abbas, L. Bih, A. Nadiri, Y. El Amraoui, D. Mezzane, B. Elouadi, J. Molec. Struct. 876(1–3) 2008 194-198.
12. F. H. ElBatal, A. M. Abdelghany, R. L. Elwan, J. Molec. Struct. 1000 (2011) 103-108.

13. F. H. ElBatal, Y. M. Hamdy, S. Y. Marzouk, *Mater. Chem. Phys.* 112 (2008) 991-1000.
14. S. Rada, E. Culea, R. Chelcea, M. Rada, A. Bot, N. Aldea, V. Rednic, *Ceramics International* 39 (2013) 1403–1411
15. L. Bih, L. Abbas, S. Mohdachi, A. Nadiri, *J. Molec. Struct.* 891 (2008) 173.
16. Baldassare Di Bartolo (Ed.), *Spectroscopy of Solid-State Laser – Type Materials*, Plenum Publishing Corporation, New York, 1987, p. 238.
17. A. A. Kaminskii, *Laser Crystals*, second ed. Springer, Berlin, 1989.
18. S. Rada, M. Culea, M. Rada, P. Pascuta, V. Maties, E. Culea, *J. Molec. Struct.* 937 (2009) 70.
19. E. I. Kamitsos, Y. D. Yianopoulos, M. A. Karakassides, G. D. Chryssikos, H. Jain, *J. Phys. Chem.* 100 (1996) 11755.
20. L. Baia, T. Iliescu, S. Simon, W. Kiefer, *J. Molec. Struct.* 599(1-3) (2001) 9.
21. M. K. Murthy, J. Ip, *Nature* 201 (1964) 285.
22. G. S. Henderson, *J. Non-Cryst. Solids* 353 (2007) 1695.
23. B. L. Shivachev, T. Petrov, H. Yoneda, R. Titorenkova, B. Mihailova, *Scripta Materialia* 61 (2009) 493.
24. G. S. Henderson, H. M. Wang, *Eur. J. Mineral* 14 (2002) 733.
25. G. Vetter, F. Queyroux, P. Labe, M. Goreaud, *J. Solid State chem.* 45(3) (1992) 293.
26. R. M. Atkins, V. Mizrahi, *Electron. Lett.* 28 (1992) 1742.
27. D. Ehrt, *J. Non-Cryst. Solids* 348 (2004) 22.
28. Z. Zhang, (1993) *Phys Chem Glasses* 34:95
29. S. B. M. Krishna, A. R. Babu, R. Sree. Ch, D. K. Rao, *J. Non-Cryst. Solids* 356 (2010) 1754-1761

30. F. Farges, R. Siewert, G. E. Brown, A. Guesdon, *Canadian Mineralogist* 44 (2006) 731-753.
31. R. J. Landry, *J. Chem. Phys.* 48 (1968) 1422-1423.
32. O. Cozar, D. A. Magdas, I. Ardelean, *J. Non-Cryst. Solids* 354 (2008) 1032-1035.
33. K. J. Rao, *Struct. Chem. Glasses* (2002) 463.
34. N. Srinivasa Rao, P. Raghava Rao, Y. Gandhi, Ch. S. Rao, G. S. Baskaran, V. R. Kumar, N. Veeraiyah, *Physica B* 406 (2011) 4494.
35. S. Rada, E. Culea, *J. Non-Cryst. Solids*, 357(7) (2011) 1724-1728.
36. S. Rada, M. Rada, E. Culea, *J. Non-Cryst. Solids* 357 (2011) 62-66.
37. M. Ferraris, D. Milanese, C. Contardi, Q. Chen, Y. Menke, *J. Non-Cryst. Solids* 347 (2004) 246.
38. D. E. Keller, T. Visser, F. Soulimani, D. C. Konigsberger, B. M. Wechuysen, *Vibrat. Spectrosc.* 43 (2007) 140.
39. X. Gao, I. E. Wachs, *J. Phys. Chem. B* 104 (2000) 1261.